JAAS

PAPER

View Article Online
View Journal | View Issue

Cite this: *J. Anal. At. Spectrom.*, 2019, **34**, 1630

A laser ablation resonance ionisation mass spectrometer (LA-RIMS) for the detection of isotope ratios of uranium at ultra-trace concentrations from solid particles and solutions

Ilya Strashnov, *[a] Igor Izosimov,[b] Jamie D. Gilmour,[c] Melissa Anne Denecke,[d] Jose Almiral,[e] Andrew Cannavan,[f] Gang Chen,[g] Champa Dissanayake,[h] Iryna Doroshenko,[i] Tibari Elghali,[j] Emma Enston,[a] Biyagamage Ruchika Fernando,[k] Gabriel Kasozi,[l] Simon Kelly,[f] Mohammed Maqsood,[a] Syahidah Akmal Muhammad,[m] Christopher Muryn,[a] Alexey L. Pomerantsev,[n] Dileep Kumar Singh,[o] Gareth Smith,[a] Fouad Taous,[j] Carole Webb,[a] David Williamson,[p] Zhenzhen Xu,[g] Shuming Yang[g] and Andreas Zitek[q]

A commercial MALDI-TOF mass spectrometer has been combined with a tunable ns-pulse laser ionisation system consisting of two dye lasers pumped by the second (532 nm) and the third (355 nm) harmonics of a Nd:YAG laser. Uranium samples in the form of solutions, suspensions or small solid grains can be placed onto an aluminium substrate without the MALDI matrix from which they are desorbed by a 337 nm nitrogen laser with a spatial resolution of ~20 μm. A rapid and simple sample preparation process not involving any chemical separation, pre-concentration or need for chemical derivatisation reactions is employed. The neutral uranium atoms and molecules are resonantly ionised by the photoionisation system. Highly selective and efficient uranium photoionisation schemes have been developed. They are three-colour, two-step photoionisation schemes involving resonance excitation from the ground state by a 424.23 nm laser (~1 μJ per pulse) and subsequently by either 578.48 nm, 575.42 nm or 574.10 nm lasers (~20 μJ per pulse) with 1064 nm (>1 mJ) ionisation into the continuum. Three-colour excitation, targeting specific uranium atomic levels, allows for selective ionisation of uranium atoms. The photo-ions have the yields of up to two orders of magnitude higher than those formed in laser desorption making them extremely suitable for the detection of isotope ratios of samples with trace concentrations. A series of measurements of reference materials with concentrations between 10^{10} and 10^{16} atoms per sample (10^{-15} to 10^{-7} g) and various isotope compositions ranging from depleted and natural to enriched uranium positively confirm the method applicability. For instance, for the samples of depleted uranium the $^{235}U/^{238}U$ < 0.003 ratio was determined with <7% precision (2σ errors) for the total uranium concentrations not exceeding ~80 fg per sample.

Received 23rd January 2019
Accepted 21st May 2019

DOI: 10.1039/c9ja00030e

rsc.li/jaas

[a]*School of Chemistry, The University of Manchester, Oxford Road, M13 9PL Manchester, UK. E-mail: Ilya.Strashnov@manchester.ac.uk*
[b]*Obedinennyj institut adernyh issledovanij, Dubna, Russia*
[c]*School of Earth Atmospheric and Environmental Science, The University of Manchester, Manchester, UK*
[d]*Dalton Nuclear Institute, The University of Manchester, Pariser Building Floor G, Manchester, M13 9PL, UK*
[e]*Department of Chemistry and Biochemistry, Florida International University, 11200 SW 8th Street, OE116 Miami, FL, USA 33156*
[f]*International Atomic Energy Agency, Joint FAO/IAEA Division of Nuclear Techniques in Food & Agriculture, Wagramer Strasse 5, P.O. Box 100, Vienna, Austria A-1400*
[g]*Chinese Academy of Agricultural Sciences, Haidian District, China 100081*
[h]*Sri Lanka Atomic Energy Board, Life Sciences Division, Colombo, Srilanka*
[i]*Faculty of Physics, Experimental Physics Department, Taras Shevchenko National University of Kyiv, Kyiv, Ukraine*
[j]*Centre National de l'Energie des Sciences et des Techniques Nucleaires, Laboratoire d'Analyses Structurales et Isotopiques (LASI), Division Exploitation des Laboratoires, Rabat, Morocco*
[k]*University of Peradeniya, Peradeniya, Central, Srilanka*
[l]*Department of Chemistry Kampala, Makerere University, Kampala, Uganda*
[m]*School of Industrial Technology/Analytical Biochemistry Research Centre Minden, Universiti Sains Malaysia, Pulau Pinang, Malaysia*
[n]*Semenov Institute of Chemical Physics RAS, Kosygin str. 4, Moscow, Russian Federation 119991*
[o]*University of Delhi, Soil Microbial Ecology and Environmental Toxicology Laboratory, Department of Zoology, New Delhi, Delhi, India*
[p]*Oxford Instruments plc, Abingdon, Oxfordshire, UK*
[q]*University of Natural Resources and Life Sciences, Tulln, Austria A-3430*

1. Introduction

Development of new physical methods for the detection of isotope ratios of small concentrations of elements in various samples is an important task in analytical science. Detection of low amounts of uranium (down to the fg-level) is of great importance due to increased requirements for environmental standards. Having been widely used in the nuclear industry uranium can be detected in many environmental samples. Infamous underground nuclear explosions at tests sites *e.g.* the "Nevada", "Semipalatinsk", and "Novaya Zemlya",[1–3] as well as radioactive waste storage facilities are environmental hazards requiring constant monitoring. In the nuclear industry, spent nuclear fuel pools serving for short-term storage of nuclear fuel rods before further reprocessing are constantly monitored for the presence of trace amounts of radionuclides. While the natural abundance of the ^{235}U isotope is <0.72%, the reactor-grade uranium can be slightly enriched to 3–5%, and enrichment of weapon-grade uranium can be >90%. Characterisation of uranium samples collected near nuclear sites based on their ^{235}U/^{238}U ratios can provide information regarding nuclear activities undertaken and potentially could serve for the goal of non-proliferation of nuclear weapons.

X-ray fluorescence analysis (typical sensitivity of 10^{-12} to 10^{-15}g) is currently widely used by industry for the detection of the elemental composition of spent nuclear fuels and environmental samples,[4] however it is not suitable for the detection of isotope ratios. Among mass spectrometry methods Inductively Coupled Plasma Mass Spectrometry (ICP-MS) that employs *e.g.* an argon plasma for the ionisation of species is widely used for the detection of isotope ratios of gas and liquid samples.[5] Solid samples can be probed in combination with laser desorption (ablation) (LA-ICP-MS).[4] Laser desorption, in turn, is widely applied to studies of biomolecules (Matrix Assisted Laser Desorption Ionisation (MALDI) method) as well as for the detection of the elemental and isotopic compositions of inorganic samples.[6] With modern development of Electrospray Ionisation (ESI) and Atmospheric Pressure Chemical Ionisation (APCI), together with MALDI and ICP-MS they are currently the leading methods most frequently used in the studies of both large organic and non-organic molecules in solutions[7] and on surfaces.[8] The main limitation of these methods is their inability to distinguish between molecular and isotopic isobars (a lack of selectivity), which complicates the analysis of trace concentrations.

Resonance ionisation mass spectrometry (RIMS) is a powerful technique that makes use of tunable lasers for resonance excitation of atoms from the ground state *via* intermediate atomic states to the ionisation continuum. Resonance laser light absorption enhances the ionisation process by several orders of magnitudes compared to non-resonant methods (*e.g.* ESI, APCI or electron impact (EI)). Moreover, because each atomic element possesses its own unique electron structure, laser beams that are tuned into specific transitions will generally selectively ionise only the atoms of interest in the sample reducing the isobaric (and isotopic, depending on the laser bandwidth) interferences. This superb sensitivity and selectivity of resonance ionisation allowed for several breakthroughs in the fields of nuclear physics[9–13] (measurement of the nuclear properties of short-lived isotopes produced in nuclear reactions) and of planetary science[14–16] (detection of isotope ratios of Kr and Xe extracted in miniature quantities from meteorites and cosmic granules – primordial chondrules).

Here we present a highly sensitive (ultra-trace level concentrations) and selective method for the detection of isotope ratios of uranium samples that can be in liquid or solid form. Laser desorption is used for sample evaporation/decomposition. Desorbed atoms are excited and ionised resonantly using three laser beams. Uranium ions are detected by a time of flight mass spectrometer with a multi-channel plate (MCP) detector.

2. Experimental setup

A Laser Ablation Resonance Ionisation Mass Spectrometer (LA-RIMS) has been developed for the detection of uranium isotope ratios. It combines a commercial high-resolution time-of-flight mass spectrometer (Bruker, Reflex III) with a photo-ionisation laser system controlled by in-house written software (see Fig. 1).

The mass spectrometer ion source is equipped with a pulsed nitrogen laser (LTB Laser technique, MNL100, ~3 ns pulse length, 337 nm wavelength, with a pulse energy of up to ~0.3 mJ per pulse). As a result of nitrogen laser light–surface interactions, a vapor cloud consisting of ions and neutral atoms is formed near the surface. Atoms are resonantly excited and ionised by the laser photo-ionisation system. Ions formed as a result of desorption and photoionisation are detected by the time of flight mass spectrometer in "linear" or "reflectron" modes using an MCP detector. A magnified image of the desorption region can be monitored using an electronic camera. Precise movement of the sample in *X*–*Y* directions with respect to the desorption laser using a pair of stepper motors is also possible. This allows for "scanning" of the sample surface with a minimum step of ~21 μm. The energy of the nitrogen (desorption) laser, and, consequently, the intensity of the desorption process, can be continuously varied with the help of an absorber of a round shape, consisting of segments of different optical densities. The photoionisation laser system consists of two tunable dye lasers (Lambda FL 2001 and Sirah), pumped, respectively, by the second (532 nm) and third (355 nm) harmonics of a solid-state Nd:YAG laser (neodymium Nd^{3+} doped in the crystal lattice of an yttrium–aluminum garnet-crystal). The Nd:YAG laser operates in the Q-switched mode.

The part of the first harmonic (1064 nm) of the Nd:YAG laser, after combining in time and space with the laser radiation from the other two lasers, is focused onto the ion source and also serves for photoionisation of atoms. The region of generation of the laser radiation of the first dye laser is ~419–430 nm (Stilbene 3 laser dye). For the second laser the Rhodamine 6G dye is used (~568–585 nm). The measurement of the wavelength is carried out by an ATOS wave meter and is displayed on the monitor screen throughout the entire measurement. The cross-section, overlap and the positions of the laser beams can be controlled using the electronic video camera which receives

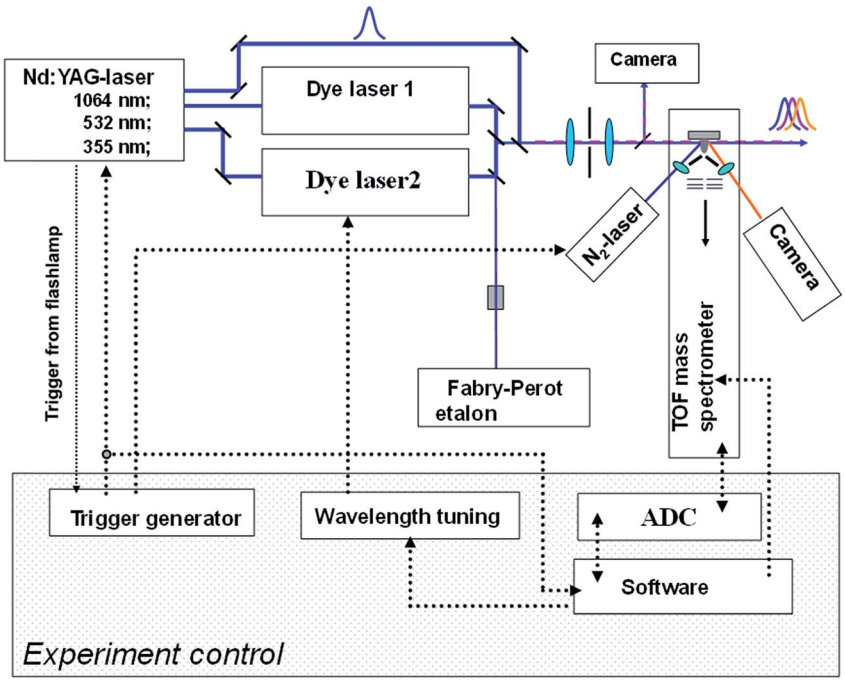

Fig. 1 Diagram of the setup for the detection of uranium isotope ratios by photoionisation mass spectrometry. The samples (solutions or solids) are placed onto a substrate from where they are desorbed with a 337 nm nitrogen laser. The neutral species are resonantly ionised by a set of tunable dye lasers pumped by a Nd:YAG laser (355 nm and 532 nm) beam. Part of the fundamental 1064 nm Nd:YAG laser beam is also used for ionisation. The photoions are detected by a TOF-mass spectrometer in linear or reflectron modes. The delay between the desorption and photoionisation pulses of ~600 ns is generated by a trigger generator which in turn is triggered by a pulse from the flash lump of the Nd:YAG laser.

a part of the laser radiation and is positioned at the same optical distance from the ion-source as the main beams. The timing diagram of the experiment is shown in Fig. 2. The time window for measurements is determined by a pulse generator (Stanford Research DG 535), whose trigger is the start time of a pulse from the Nd:YAG laser flash-lamp operating at 20 Hz. Measurements are carried out at a frequency of 4 Hz, so only every fifth pulse from the flash lamp is received by the pulse generator. Another trigger signal is generated 402.4 μs after receiving the signal from the flash lamp and is used to start the nitrogen laser. After 600 ns, another trigger signal is fed to the Q-switch input of the Nd:YAG laser and the laser pulses (1064 nm, 532 nm and 355 nm) are formed to pump dye lasers. The same trigger signal serves to start the ADC. Time-of-flight mass spectrometer settings (voltage setting of the detector and accelerating electrodes, vacuum system, repositioning and sample replacement, varying the energy of the desorbing laser, *etc.*), ADCs and video cameras are controlled by a computer program in the UNIX operating system. The laser wavelength can be tuned in small steps of ~300 MHz and controlled by the software. The ion source, the time-of-flight cavity of the spectrometer and the detector are in a vacuum of 10^{-6} to 10^{-7} mbar.

3. Sample preparation and spatial resolution

The samples are placed onto a substrate from which they are desorbed with the nitrogen laser after drying. Although being completely different, this approach is more robust compared to *e.g.* atmospheric pressure ion sources (ESI, APCI, *etc.*) employing small diameter capillaries for direction/formation of liquid sprays. Special attention to these "electrospray" sources is required at the sample preparation stage which, if not careful, could cause blockages and signal suppression due to *e.g.* high salt concentrations or presence of reactive species in solution.

The sample preparation of LA-RIMS is somewhat similar to that of MALDI except that the organic matrix is not used. In the case of MALDI, for liquid samples, a typical sample volume <1 μl is placed onto a stainless steel substrate and evaporated to dryness. An alternative to a standard stainless steel substrate was investigated. Several-mm thin plates of glassy carbon "Sigradur® G" purchased from HTW were found to be promising due to their purity, high melting point and good absorption of ultraviolet radiation in the vicinity of 337 nm, in this sense playing a role of the matrix. Small granules (~10 μm) can be prepared and dried in the form of suspensions in *e.g.* isopropanol, and can also be deposited onto synthetic graphite. Larger samples can be glued to the aluminum substrate using conductive silver glue; while the main limitation is their height <2 mm, they can be in principle up to several cm wide. In Fig. 3, the photo of the sample target is presented. Here the in-house made aluminum MALDI plate is modified with glassy carbon pieces with ~0.1 mm deep wells drilled at the surface with uranium solutions deposited and dried (c), uranium foil used in optical spectroscopy experiments (a) and small pieces of other (stainless steel) materials glued to the substrate (b), and

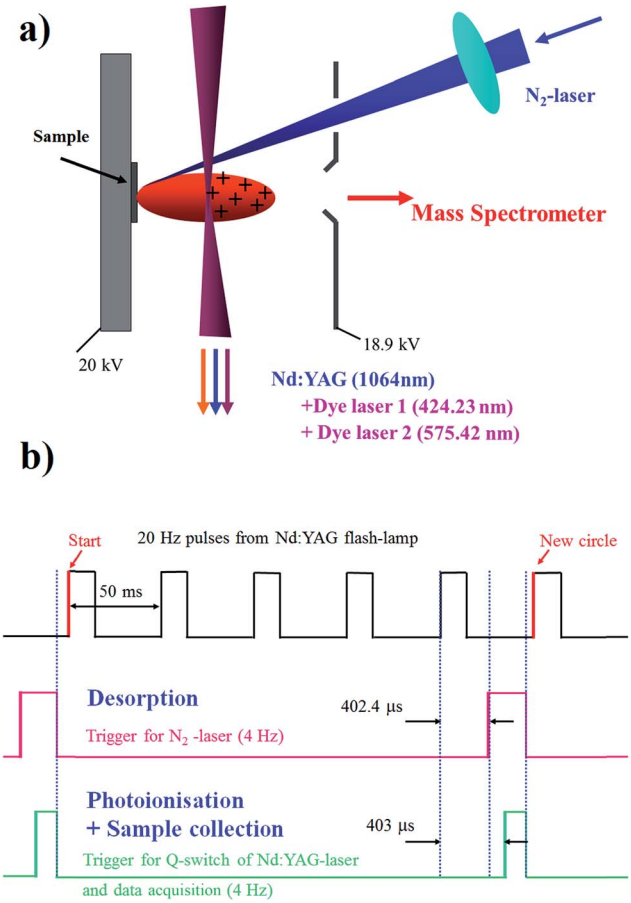

Fig. 2 Diagram of the laser ion source (a) and the timing diagram of the experiment (b). The sample material is placed at the stainless steel substrate. The desorption with a focused nitrogen laser is used to ablate the sample material from the surface. The photoionisation beams are overlapped and adjusted parallel to the surface at the distance of <1 mm. The produced ions are extracted through a conical extraction electrode having a negative potential difference of −1.1 kV with respect to the target (kept at +20 kV). The photoionisation pulses delayed ~600 ns with respect to desorption. The nitrogen laser beam repetition rate is 4 Hz and that of the Nd:YAG laser is 20 Hz which make it possible to overlap the desorption-photoionisation pulses in time with necessary delay (every 5th Nd:YAG pulse is missed).

uranium-rich granules in the form of isopropanol suspension can be seen as well deposited on the Sigradur® G substrate (d).

The spatial resolution of a method is very important especially in analysis of solid samples. The spatial resolution can be regarded as the smallest distance between points "*a*" and "*b*" of the sample at which the signal can be detected without interference from each other.

To determine the spatial resolution we have prepared a glass plate and deposited a thin (<1 μm) graphite layer by electroheating of a small piece of glassy carbon to a high temperature (~2000 C) in a vacuum. The desorption laser was fired (5–10 shots were made at each spot) and the thin graphite layer evaporated making the desorption craters visible. The sample holder was moved with the smallest steps of the stepper motor and the plate was later studied under an optical microscope. The laser fluence was increased to 0.5 J cm^{-2} from

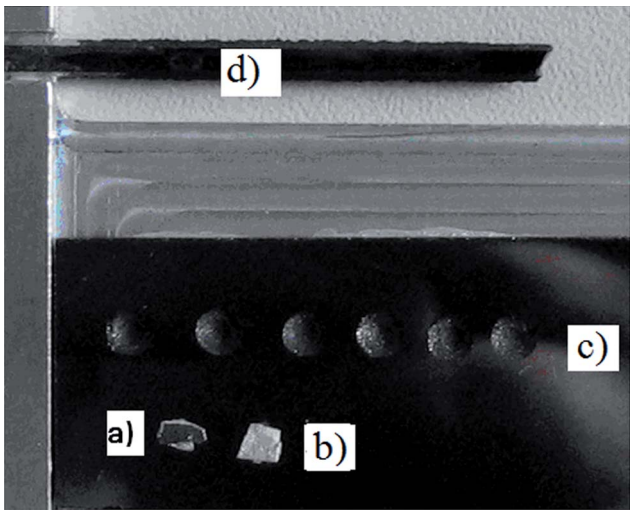

Fig. 3 An aluminum sample holder (12 × 8 cm) with a synthetic carbon plate mounted on top of it. A large solid sample *e.g.* uranium foil (a) and st. steel foil (b) can be glued with conductive silver glue. A smaller grain sample in the form of suspensions and uranium solutions can be placed into one of the wells drilled at the surface of the carbon plate (c). Different small plates of the carbon materials can also be glued to the aluminum plate and serve as a mass spec. reference (d).

usual 0.1 J cm^{-2} in order to increase the crater visibility. In Fig. 4 the optical image of the desorption craters is presented. The ellipsoidal form of the craters can be explained by the desorption beam positioned at an angle to the surface of the target. The diameter of the craters is <5 μm and the distance between the craters is ~20 μm corresponding to the minimum step with which the sample can be moved by the electric motors with respect to the desorption laser beam. This smallest distance of ~20 μm can be regarded as the spatial resolution of the method.

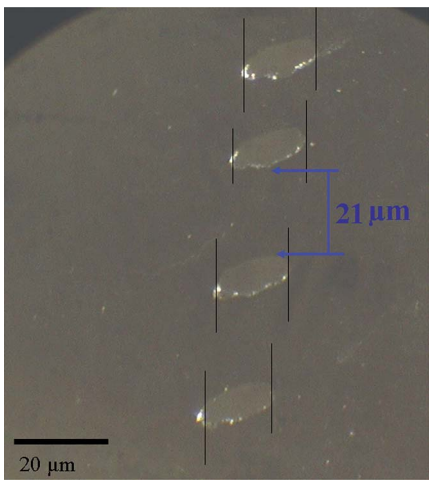

Fig. 4 An optical microscopy image of the desorption craters. The craters from the nitrogen 337 nm laser are visible at the surface of the glass plate covered with a thin layer of carbon. The plate can be moved with stepper motors in precision steps of ~21 μm with respect to the desorption laser. This constitutes the spatial resolution of the method.

4. Laser desorption process and estimation of the amount of desorbed matter

Laser desorption is a process of removal of material from the surface of a sample as a result of interaction with laser irradiation.[17,18] The dimensions of desorption craters depend on the laser wavelength, fluence, and pulse duration as well as the ability of a sample to absorb laser radiation of a certain wavelength.

During desorption with femtosecond and picosecond laser pulses of small fluences (<1 J cm^{-2}), desorption craters have a smaller diameter size (<1 μm) compared to those formed during ns-pulses. At higher fluences (>1 J cm^{-2}) the sizes of craters become comparable.

During desorption with ns-lasers the sample surface is heated, melted, and the sample material evaporates. With increasing laser fluence to 1 J cm^{-2}, a gradual transition from the "normal evaporation" phase of the material to the "normal boiling" phase is observed. For large fluences (>1 J cm^{-2}), desorption enters the so-called "explosive boiling" phase, with the formation of deep irregular craters and melted edges. Desorption in this phase is called "laser ablation".[19–22]

In the case of our uranium measurements the typical fluence of the 337 nm laser is 0.2 J cm^{-2}, corresponding to the "normal evaporation" phase. The process of melting of a sample material can be described by a simple thermodynamic formula:

$$\Delta E_{\text{melt.}} = V_{\text{melt.}}(C\rho[T_{\text{melt.}} - 239\ \text{K}] + H_{\text{melt.}}\rho), \quad (1)$$

where ΔE is the energy required to melt the sample material, $V_{\text{melt.}}$ is the volume of the evaporation zone, C is the heat capacity of the sample, ρ is the density, $T_{\text{melt.}}$ is the melting point, and $H_{\text{melt.}}$ is the heat of fusion.

In Fig. 5 a scanning electron microscopy (SEM) image of a desorption crater formed at the surface of the graphite substrate after 100 pulses of the 337 nm laser with ~0.4 J cm^{-2} fluence is presented. The area of the melting zone determined from the image is ~30 μm × 20 μm. If we neglect the dissipation of energy in the melting region, as well as the reflection of light from the sample surface, then the average depth of the melting zone can be estimated using formula (1): (ρ = 3.5 g cm^{-3}, $T_{\text{melt.}}$ = 3820 K, $H_{\text{melt.}}$ = 105 kJ mol^{-1}, C = 720 J kg^{-1} K^{-1}) as ~7 μm. Thus, with a laser fluence of 0.4 J cm^{-2} after 100 laser pulses the mass of evaporated graphite is ~15 pg. Depending on the sample material, this number gives an indication of the method sensitivity during desorption of uranium from the solid samples.

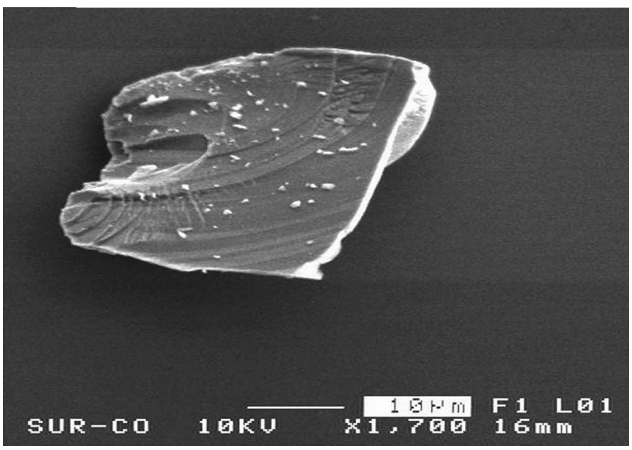

Fig. 5 A scanning electron microscopy (SEM) image of a desorption crater at the graphite substrate formed at the surface after 100 pulses of the 337 nm laser with ~0.4 J cm^{-2} fluence. The area of the melting zone determined from the image is ~30 μm × 20 μm.

5. Resonance photoionisation of desorbed uranium atoms and selectivity

The important step in the development of the RIMS method is the search for effective and selective photoionisation schemes. In uranium photoionisation experiments, uranium foil was used as a target. Initially only the first UV laser on Stilbene 3 dye was scanned with a step of ~1 GHz (7.3 × 10^{-4} nm) and the photosignal was continuously recorded with a time-of-flight mass spectrometer. Such "a single colour" photoionisation scheme employs the same two UV photons with the total energy exceeding the ionisation potential of the uranium atom. The second Rhodamine 6G dye laser was scanned at a later stage at which the second step uranium transitions from the excited states found previously were recorded. Finally, the 1064 nm Nd:YAG beam was overlapped with the dye laser beams and the photoionisation schemes were complete. The most effective photoionisation schemes found during these experiments are presented in Fig. 6.

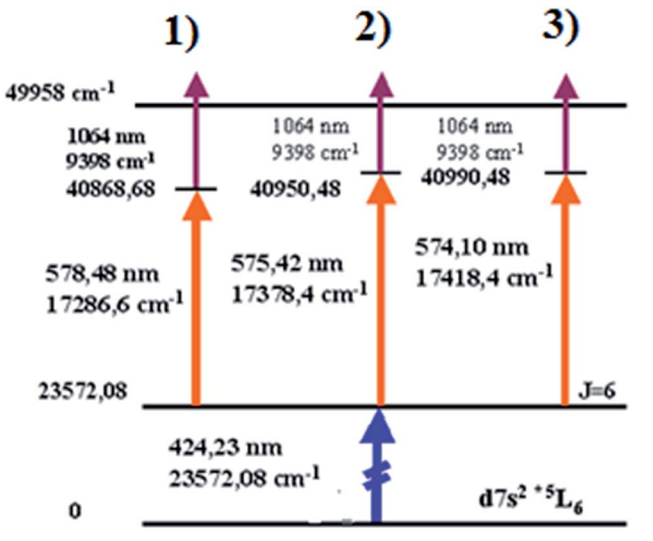

Fig. 6 Most efficient uranium photoionisation schemes. The first UV transition dye laser works on Stilbene 3 (~1 μJ per pulse) followed by the second transition excited by the dye laser on Rhodamine 6G (~20 μJ per pulse). A part of the fundamental 1064 nm radiation from the Nd:YAG laser (~1 mJ per pulse) ionises atoms into the continuum.

In these three-colour photoionisation schemes, the first resonant transition ($\lambda = 424.23$ nm) from the ground state ([Xe] $5f^3 6d^7 s^2\ ^5L_6$) is excited by a Stilbene 3 dye laser with a pulse energy of ~ 1 μJ. A Rhodamine 6G dye laser (pulse energy ~ 20 μJ) was used to excite the second resonant transitions ($\lambda =$ 578.48 nm, $\lambda = 575.428$ nm, $\lambda = 574.10$ nm). The Nd:YAG laser ($\lambda = 1064$ nm, 1 mJ) brings the atoms into the ionisation continuum.

The selectivity of the photoionisation schemes is related to the resonance signal enhancement. Depending on the laser power at each step, this can be defined as a ratio of the magnitude of the signal from resonantly ionised uranium to the signal from non-resonantly ionized uranium. The resonance wavelength scan of the first and second transitions is presented in Fig. 7. Note that in the case of the scan of the first UV transition the laser power was increased to allow for the efficient ionisation of the atoms leading to an increase in non-resonance UV ionisation. Nevertheless, signal enhancements for the second transitions are $S_1 = 27$, $S_2 = 32$, $S_3 = 18$ for the three schemes respectively with a factor of 2 enhancement at the first step.

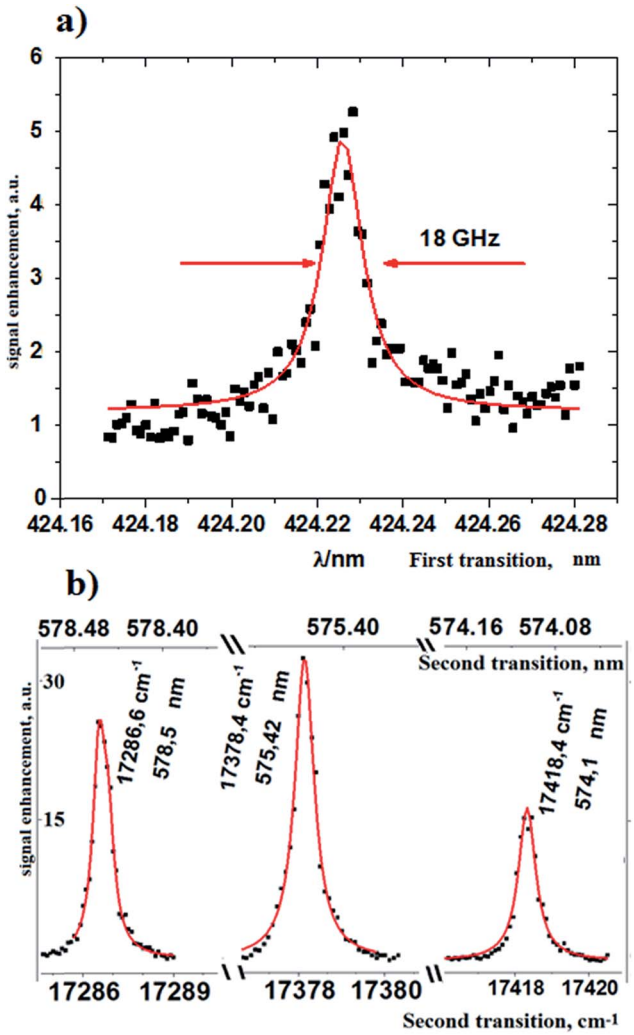

Fig. 7 Wavelength scans of the first (a) and the second (b) uranium atomic transitions. The photoionisation signal enhancement (~an order of magnitude on the first and ~2 orders of magnitude on the second transition) compared to non-resonant background (when the laser wavelength is detuned from the wavelength of the transition) pushes the method sensitivity to a high level making analysis of uranium isotope ratios at the fg level possible.

6. Measurement of uranium isotope ratios and sensitivity of the method

Detection of uranium isotope ratios is challenging due to large ^{238}U abundances and several orders of magnitude lower abundances of ^{234,235}U isotopes. In some cases, it is important to determine whether uranium samples have a natural composition ($^{235}U/^{238}U \sim 0.007$) or contain some fractions of enriched ^{235}U (up to several %) or depleted uranium (typically $^{235}U/^{238}U \sim 0.003$). This need often arises in test laboratories providing control for unauthorized nuclear activities.[23,24] If the fraction of enriched (or depleted) uranium in the bulk natural samples is small then the $^{235}U/^{238}U$ ratio will only slightly differ from the value of already "small" isotopic ratios of natural uranium.[25]

In our test experiments the measurement of "small" isotope ratios was carried out using certified reference samples obtained from the Institute for Reference Materials and Measurements (IRMM), Belgium (samples IRMM-183*, IRMM-3184*, IRMM-3185*, IRMM-3186*, IRMM-3187*). The total uranium content in the samples was $\sim 5 \times 10^{13}$ atoms. To account for the systematic instrumental errors mainly caused by isotope fractionation arising during laser ablation and possible differences in the ionisation efficiencies of the ^{235}U isotope having non-zero nuclear spin, we adopted a strategy developed during our previous studies.[26–33] The samples were measured by comparison to standard samples having natural composition,

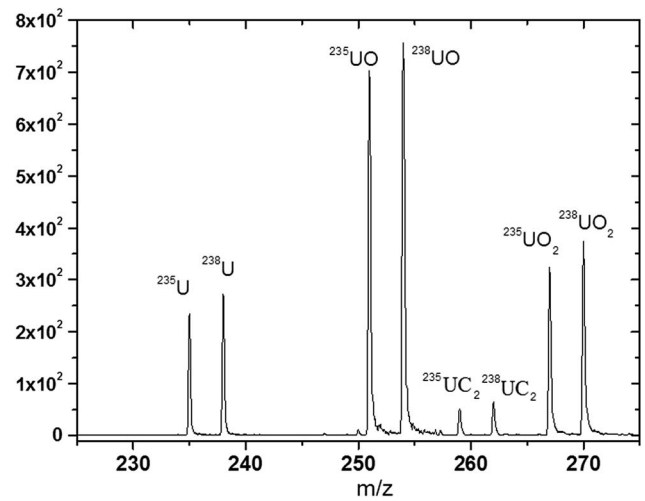

Fig. 8 A time of flight mass spectrum (~10^8 molecules) of the enriched uranium in methanol solution. The photoionisation of atomic uranium is performed in a three-colour scheme employing 242.23 nm, 575.42 and 1064 nm laser beams. Resonant enhanced photoions of abundant UO, UO_2 species and UC_2, formed as a result of laser driven surface chemistry on the graphite substrate, can be seen.

Table 1 Isotope ratios of reference uranium standards having different ^{235,238}U isotope compositions detected by the photoionisation mass spectrometry method. Total uranium content of the samples is 5 × 10^{13} atoms

	^{235}U/^{238}U reference standard value[29]	^{235}U/^{238}U photoionization method
1	0.047326(35)	0.0492(20)
2	0.030786(22)	0.0328(13)
3	0.020062(15)	0.02101(11)
4	0.0072617(51)	0.00715(54)
5	0.0032169(20)	0.00332(36)

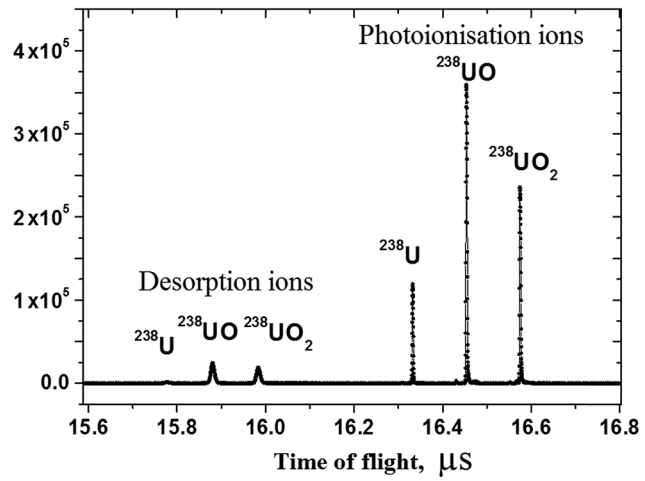

Fig. 9 Comparison of the ionisation efficiencies of photoionisation with the desorption ionisation method (similar to MALDI). The 337 nm laser "desorption ion" abundances are up to several orders of magnitude lower compared to "photoionisation ions" arriving 600 ns later in the time of flight spectrum. The mass resolution is also better in the case of photoionisation, because of the tight focus of the laser beam in the ionisation region (<1 mm above the surface of the sample holder).

the correction factors were calculated for each isotope, and the determined isotope ratios values were calculated at the data analysis stage by determining the area of the peaks (the total correction for instrumental errors was <5%). The magnitude of systematic errors and the effect of differences in ionisation efficiencies of ^{235}U and ^{238}U on detected isotope ratio values can be seen from Fig. 8 where a mass spectrum of the enriched ~1 : 1 uranium solution is presented. The measurement results of the 5 reference samples with isotope ratios varying from depleted (^{235}U/^{238}U = 0.0032) to slightly enriched uranium (^{235}U/^{238}U = 0.047) are presented in Table 1. The errors, that are 2σ errors, are calculated from 10 repeat measurements and do not exceed 7%.

During UV laser ablation, some uranium species become ionized. In this respect switching to an IR laser producing a smaller amount of desorption ions and more neutrals will be more preferable. The sensitivity of the photoionisation method is higher than those of laser desorption methods (*e.g.* MALDI). A TOF mass spectrum of a natural uranium solution is presented in Fig. 9. The first group is the desorption ions followed by several orders of magnitude more abundant photoionisation species. Uranium oxides are the most abundant in solution and the desorption signal from atomic uranium is low abundant. By examining the photoionisation process one can notice (in addition to overall several orders of magnitude higher abundances of the photoionisation species) a significant resonance enhancement of the atomic photoionisation signal compared to oxides. This signal, albeit less abundant, has less probability to be contaminated with atomic/molecular isobars.

The purpose of the next experiments was to determine the minimum level of uranium concentrations at which the measurements of the isotope ratios would have meaningful results. The atomic photoionisation signal was used for the calculation of ^{235}U/^{238}U ratios of samples having different concentrations (5 × 10^8 to 5 × 10^{16} atoms per sample or 8 × 10^{-16} to 8 × 10^{-8} g per sample, natural uranium composition).[34] The measurement results are presented in Table 2. The isotope ratios were determined with errors not exceeding 10% (2σ errors) for uranium concentrations down to 5 × 10^{10} atoms per sample (or ~80 fg per sample). Below this level only a qualitative analysis is possible, mainly due to the data acquisition system constraints. The dynamic range of the digitizer card does not allow efficient detection of ^{235}U in the presence of the ^{238}U signal at low voltage scales. Upgrading the digitizer card with a higher bit rate and developing software allowing alternating acquisition between a higher voltage scale for ^{238}U and a smaller one for ^{235}U ("a voltage scale switching")

Table 2 Isotope ratios of natural uranium detected with the photoionisation mass spectrometry method. A sub-fg detection limit (^{235}U) has been determined using uranium methanol solutions having concentrations varying by several orders of magnitude. At these low level concentrations the measurement of meaningful isotope ratios is still possible with the precision of <7% (2σ errors)

	Total U content, atoms per sample	Amount of desorbed U, atoms per laser area	^{235}U content, g per sample	^{238}U content, g per sample	Experimental ratios, ^{235}U/^{238}U
1	5 × 10^8	10^6	6 × 10^{-18}	8.24 × 10^{-16}	Qualitative analysis
2	5 × 10^9	10^7	6 × 10^{-17}	8.24 × 10^{-15}	Qualitative analysis
3	5 × 10^{10}	10^8	6 × 10^{-16}	8.24 × 10^{-14}	0.00752(91)
4	5 × 10^{11}	10^9	6 × 10^{-15}	8.24 × 10^{-13}	0.00731 (68)
5	5 × 10^{13}	10^{11}	6 × 10^{-13}	8.24 × 10^{-11}	0.00702 (57)
6	5 × 10^{15}	10^{13}	6 × 10^{-11}	8.24 × 10^{-9}	0.00692 (41)
7	5 × 10^{16}	10^{14}	6 × 10^{-10}	8.24 × 10^{-8}	0.00718 (30)

could allow for the detection of isotope ratios at much smaller concentrations.

7. Conclusions

A commercial laser desorption time of flight mass spectrometer (Bruker Reflex 3) has been equipped with a laser ionisation system consisting of two tunable dye lasers pumped with 355 & 532 nm Nd:YAG lasers. Resonance excitation of uranium atoms from the ground state *via* intermediate exciting states followed by ionisation into the continuum by a 1064 nm beam is an efficient and isobarically selective way of producing ions from atomic plumes under vacuum conditions. Resonantly enhanced ion yields are up to 2 orders of magnitude higher compared to *e.g.* desorption ionisation methods similar to MALDI, not only for the atomic but also for abundant molecular species.

Sample preparation involving the use of aluminium, stainless steel or synthetic graphite substrates (in this case playing the role of the "matrix") for dried solutions, suspensions of small particles and solid samples glued to the substrate is simple and does not include chemical separation and preconcentration, and unlike GCMS analysis it does not involve the use of chemical derivatisation reactions. The sample material is desorbed from the surface with a spatial resolution of 21 μm and the neutrals are ionised ~600 ns later by the laser system.

The isotope ratios can be determined for samples containing trace concentrations of uranium effectively distinguishing between *e.g.* natural, reactor or weapon-grade uranium. For instance, for the samples of depleted uranium having a small $^{235}U/^{238}U = 0.003$ ratio it is possible to determine this ratio with <7% precision (2σ errors) for the total concentrations not exceeding 80 fg per sample.

Conflicts of interest

There are no conflicts to declare.

Acknowledgements

This work was supported by the STFC GCRF fund [grant number ST/R002681/1].

References

1 T. B. Cochran, *et al.*, *U.S. Nuclear Warhead Production*, John Wiley Press, 1987.
2 D. Holloway, *The Soviet Union and the Arms Race*, Cambridge University Press, 2nd edn, 1984.
3 T. B. Cochran, *Soviet Nuclear Weapons*, Ballinger Pub Co, 1989.
4 K. Janssens, *et al.*, *Microscopic X-ray Fluorescence Analysis*, Wiley, 2000.
5 T. R. Ireland, Recent developments in isotope-ratio mass spectrometry for geochemistry and cosmochemistry, *Rev. Sci. Instrum.*, 2013, **84**(1), 011101.
6 R. E. Russo, *et al.*, *Anal. Chem.*, 2002, **74**(3), 70A–77A.
7 M. Karas and F. Hillenkamp, *Anal. Chem.*, 1988, **60**, 2299.
8 K. Tanaka, *Angew. Chem., Int. Ed.*, 2003, **42**(33), 3860–3870, The Origin of Macromolecule Ionization by Laser Irradiation.
9 I. Budinčević, *et al.*, *Phys. Rev. C: Nucl. Phys.*, 2014, **90**(1), laser spectroscopy of francium isotopes at the borders of the region of reflection asymmetry.
10 K. M. Lynch, *et al.*, *Phys. Rev. X*, 2014, 011055. Decay-assisted collinear resonance ionisation spectroscopy: application to neutron-deficient francium.
11 K. T. Flanagan, *et al.*, *Phys. Rev. Lett.*, 2013, **111**, 212501, collinear resonance ionization spectroscopy of neutron-deficient francium isotopes.
12 T. E. Cocolios, *et al.*, *Nucl. Instrum. Methods Phys. Res., Sect. B*, 2013, **317**, 565–569, the collinear resonant ionisation spectroscopy (CRIS) experimental setup at CERN-ISOLDE.
13 K. T. Flanagan, *et al.*, *Hyperfine Interact.*, 2013, **227**(1–3), 131–137, first results from the CRIS experiment.
14 I. Strashnov and J. D. Gilmour, *Meteorit. Planet. Sci.*, 2013, **48**(12), 2430–2440, ^{81}Kr–Kr cosmic ray exposure ages of individual chondrules from Allegan.
15 I. Strashnov and J. D. Gilmour, *Hyperfine Interact.*, 2014, **227**(1–3), 259–270, resonance ionisation mass spectrometry of krypton and its applications in planetary science.
16 I. Strashnov, *et al.*, *Geochim. Cosmochim. Acta*, 2012, **106**, 71–83. Time of impacts that deliver samples of Vesta to Earth derived from ultrasensitive ^{81}Kr–Kr cosmic ray exposure age analysis of eucrites.
17 R. F. Haglung, *Appl. Surf. Sci.*, 1996, **96–98**, 1–13, microscopic and mesoscopic aspects of laser-induced desorption and ablation.
18 D. Martin, *et al.*, *Surf. Sci.*, 2003, L151–L157. Site-selective, resonant photochemical desorption of metal atoms with laser light: manipulation of metal surfaces on the atomic scale.
19 R. Srinivasan, *et al.*, *Pure Appl. Chem.*, 1990, **62**(8), 1581–1584. Ultraviolet laser ablation and decomposition of organic materials.
20 M. Ye, *et al.*, *J. Appl. Phys.*, 2001, **89**, 5183, time-of-flight and emission spectroscopy study of femtosecond laser ablation of titanium.
21 J. Díaz, *et al.*, *J. Appl. Phys.*, 1998, **84**, 572. Role of the plasma in the growth of amorphous carbon films by pulsed laser deposition.
22 R. Stoian, *et al.*, *Opt. Eng.*, 2005, **44**, 051106. Temporal pulse manipulation and consequences for ultrafast laser processing of materials.
23 C. Jaeger, Joint US/Russian Plutonium Disposition Study, *Nonproliferation Issues, 37th Annual Meeting Proceedings of the Institute of Nuclear Material Management*, Naples, Florida, 1996, pp. 884–889.
24 D. Albright, F. Berkhout, and W. Walker, *World Inventory of Plutonium and Highly Enriched Uranium*, SIPRI, 1993.
25 M. Magnoni, *et al.*, *Radiat. Prot. Dosim.*, 2001, **97**(4), 337–340, variations of the isotopic ratios of uranium in environmental samples containing traces of depleted uranium.

26 I. Strashnov, *et al.*, *J. Anal. At. Spectrom.*, 2011, **26**, 1763–1772. A resonance ionization time of flight mass spectrometer with cryogenic sample concentrator for isotopic analysis of krypton from extraterrestrial samples.
27 I. Strashnov, *et al.*, *Appl. Phys. B: Lasers Opt.*, 2010, **99**, 3. Controlling isotopic effects in the resonance ionisation mass spectrometry of krypton.
28 I. Strashnov, *et al.*, *Opt. Commun.*, 2009, **282**, 3487–3492. Hyperfine structure induced isotopic effects in krypton resonance ionization mass spectrometry.
29 J. Maul, T. Berg, *et al.*, *Nucl. Instrum. Methods Phys. Res., Sect. B*, 2004, **226**, 4. A laser desorption/resonance enhanced photoionisation TOF-system for the spatially resolved trace analysis of elements.
30 I. Strashnov, *et al.*, *Opt. Commun.*, 2009, **282**(5), 966–969, tunable VUV light generation for resonance ionization mass spectrometry of krypton.
31 A. Andrighetto, *et al.*, *Eur. Phys. J. A*, 2004, **19**(3), 341–345. Photon- and neutron-induced fission on uranium carbide target.
32 J. Maul, *et al.*, *Opt. Commun.*, 2005, **256**(4–6), 364–372. Multi-color resonance ionization of laser ablated gadolinium at high laser power.
33 J. Maul, *et al.*, *Anal. Bioanal. Chem.*, 2006, **386**(1), 109–118. Spatially resolved ultra-trace analysis of elements combining resonance ionization with a MALDI-TOF spectrometer.
34 Institute for Reference Materials and Measurements, Isotopic Reference Materials Certified by IRMM (Belgium), Catalog 2004–2005.